MNRAS **448,** 3820–3828 (2015) doi:10.1093/mnras/stv278

Thermal H/D exchange in polar ice – deuteron scrambling in space

T. Lamberts,[1,2]★ S. Ioppolo,[2] H. M. Cuppen,[2] G. Fedoseev[1] and H. Linnartz[1]

[1]*Raymond and Beverly Sackler Laboratory for Astrophysics, Leiden Observatory, Leiden University, PO Box 9513, NL-2300 RA Leiden, the Netherlands*
[2]*Faculty of Science, Radboud University Nijmegen, IMM, PO Box 9010, NL-6500 GL Nijmegen, the Netherlands*

Accepted 2015 January 29. Received 2015 January 14; in original form 2014 November 28

ABSTRACT

We have investigated the thermally induced proton/deuteron exchange in mixed amorphous H_2O:D_2O ices by monitoring the change in intensity of characteristic vibrational bending modes of H_2O, HDO, and D_2O with time and as function of temperature. The experiments have been performed using an ultrahigh vacuum setup equipped with an infrared spectrometer that is used to investigate the spectral evolution of homogeneously mixed ice upon co-deposition in thin films, for temperatures in the 90–140 K domain. With this non-energetic detection method, we find a significantly lower activation energy for H/D exchange – 3840 ± 125 K – than previously reported. Very likely this is due to the amorphous nature of the interstellar ice analogues involved. This provides reactive time-scales ($\tau < 10^4$ yr at $T > 70$ K) fast enough for the process to be important in interstellar environments. Consequently, an astronomical detection of D_2O will be even more challenging because of its potential to react with H_2O to form HDO. Furthermore, additional experiments, along with previous studies, show that proton/deuteron swapping also occurs in ice mixtures of water with other hydrogen-bonded molecules, in particular on the OH and NH moieties. We conclude that H/D exchange in ices is a more general process that should be incorporated into ice models that are applied to protoplanetary discs or to simulate the warming up of cometary ices in their passage of the perihelion, to examine the extent of its influence on the final deuteron over hydrogen ratio.

Key words: astrochemistry – solid state: volatile – methods: laboratory: molecular – ISM: molecules.

1 INTRODUCTION

The delivery of water to Earth is far from understood. Several hypotheses have been put forward, among which delivery by comets and/or asteroids during the so-called late veneer stage (Morbidelli et al. 2000; Cleeves et al. 2014), direct adsorption of water on to grains prior to planetary accretion (Muralidharan et al. 2008), and in the recent 'Grand Tack' model, water delivery during the formation phase of terrestrial planets (O'Brien et al. 2014). Since the ratio between deuterons and protons incorporated in water molecules is elevated in the Earth Ocean with respect to that of the initial bulk solar composition, the D/H fraction in various molecules is a logical tracer for the proposed origins. This concerns particularly the ratio of HDO over H_2O. The D_2O abundance is expected to be low, because the amount of deuterium present in the interstellar medium is a factor 100 000 less than that of hydrogen. In fact the number of astronomical D_2O detections is very limited: in the cold envelope layer surrounding solar-type protostar IRAS 16293−2422 (Butner et al. 2007; Vastel et al. 2010; Coutens et al. 2013) and in the warmer regions surrounding the Class 0 protostar NGC 1333 IRAS2A (Coutens et al. 2014).

It should be noted, though, that a direct comparison of observed D/H ratios between different locations may be a too naive approach to identify the origin of our water, as obviously a number of processes are at play that may scale differently over time for different conditions. For example, investigating molecules other than water, it has been found that deuterium fractionation in low-mass protostellar envelopes and molecular outflows for H_2CO and CH_3OH are higher than those for H_2O and NH_3 as summarized in fig. 11 by Caselli & Ceccarelli (2012). This difference is argued to reflect the temporal sequence in which the species are formed, as with decreasing gas-phase CO (increasing frozen out solid CO) abundances the gas-phase atomic D/H ratio is found to increase. Final values may also be different in different environments, e.g. low- versus high-mass protostellar envelopes. In order to interpret molecular D/H ratios correctly, it is important to investigate all impacting processes. In the past, the focus has been on isotope-dependent gas-phase chemical processes. So far, the two main routes are first gas-phase isotope-dependent reactions with H_2D^+ transferring its deuterium atom and second the enhanced gas-phase D/H ratio after CO freeze-out that impacts on ice chemistry by the higher probability of deuterium

★ E-mail: lamberts@strw.leidenuniv.nl

deposition (Tielens 1983; Caselli & Ceccarelli 2012). In the solid state, on the grains, deuterium fractionation is further determined by the chemical surface reaction networks. These involve both hydrogenation and deuteration pathways and the crosslinks between them. This paper focuses in detail on one particular process only: thermally induced proton/deuteron exchange reactions in the ices.

In general, the grain temperature during the formation of the icy mantles in the dense and dark regions of the interstellar medium is low, between 10 and 20 K (Bergin & Tafalla 2007). The exact temperature determines the surface reaction routes taken, by, e.g. sticking coefficients and the relative importance of tunnelling transmission coefficients, that lead eventually to the formation of species like CH_3OH and H_2O (Hiraoka et al. 1998; Watanabe & Kouchi 2002; Ioppolo et al. 2008; Miyauchi et al. 2008; Fuchs et al. 2009). At later evolutionary stages in the star-forming sequence, surface temperatures are no longer homogeneously distributed throughout the core or disc and can range up to 100 K (van der Tak et al. 2000; Aikawa et al. 2002; Jørgensen, Schöier & van Dishoeck 2002; Nomura & Millar 2005; Bergin & Tafalla 2007; Launhardt et al. 2013). At 100 K, ices are expected to have been fully evaporated, thus transferring molecules from the grains to the gas phase.

Within the astrochemical community, proton exchange in polar (i.e. water-rich) ices has attracted special attention. In the context of ion formation at low and higher temperatures, Grim et al. (1989) discuss the proton hopping between the hydrogen-bonded molecules leading to the formation of NH_4^+ and OCN-. As stated by Tielens (2013) heating and sublimation seem to be important in interstellar ices near young stars in modelling the warm gas; non-energetic thermal reactions may therefore be relevant as well. Proton exchange can be important in particular since the main component of ices is H_2O and, moreover, the main reservoir of deuterium is HDO (Rodgers & Charnley 2002). If indeed such a scrambling of protons and deuterons occurs efficiently, this implies that not the low-temperature reaction routes are decisive for final HDO/H_2O ratio, but rather the total number of H and D atoms incorporated in hydrogen-bonded molecules. Ratajczak et al. (2009) showed that the hydroxyl group in a methanol molecule exchanges its proton or deuteron with surrounding water molecules and proposes this as one of the possible explanations for the deviation between modelled and observed CH_2DOH/CH_3OD ratios (Ratajczak et al. 2011).

Interstellar or circumstellar ices and cometary ices are thought to have a common chemical origin (Bockelée-Morvan et al. 2000), but the temperature processing of ices in comets is of an intrinsically different nature. Ices are typically much thicker, i.e. orders of magnitude compared to the layer thicknesses of several tens of monolayers typical for interstellar ices. Moreover, each passage through the perihelion can have a large impact on the temperature depending on the distance to the central object. In the cometary community, however, H/D exchange is often modelled only in the coma gas-phase chemistry via several reactions (Rodgers & Charnley 2002) following sublimation of ices.

The mechanisms underlying proton/deuteron scrambling have already been studied extensively in the 1980's in the physical chemical community, in particular by Devlin and co-workers (Thornton, Khatkale & Devlin 1981; Bertie & Devlin 1983; Collier, Ritzhaupt & Devlin 1984; Wooldridge & Devlin 1988) who studied H/D exchange in water ices as well as water–ammonia mixtures with different isotopic compositions. For the case of water ice, exchange has been found to occur both in the bulk (Collier et al. 1984) and on the surface (Uras-Aytemiz, Joyce & Devlin 2001; Park, Jung & Kang 2004; Moon, Yoon & Kang 2010). In the case of isolated D_2O molecules in a H_2O environment, the prevailing mechanism is often referred to as the so-called hop-and-turn mechanism. In Fig. 1, three scenarios of the local ice structure are depicted: (a) a perfect crystalline structure, (b) an ionic defect, i.e. the presence of H_3O^+, and (c) an L-defect, i.e. the lack of an expected hydrogen bond. Under influence of an ionic defect, the heavy water is converted into two coupled HDO entities that share a hydrogen bond. These can be converted into two nearest-neighbour HDO molecules by passage of an L-defect. Finally, two isolated molecules are created after an additional proton transfer. Such a detailed mechanism, with corresponding distinct infrared (IR) spectra (in the O–D stretching region) cannot be resolved for current astronomical IR spectra. For astrochemical purposes, the overall reaction can therefore be summarized as

$$H_2O + D_2O \xrightarrow{k_f} 2HDO \quad \text{(R1)}$$

$$2HDO \xrightarrow{k_f} D_2O + H_2O. \quad \text{(R2)}$$

Collier et al. (1984) and Wooldridge & Devlin (1988) studied cubic ices with D_2O concentrations of several per cent in a high vacuum setup. The activation energy for proton exchange was found to be ∼5000 K, which means that the process is not likely to be relevant on interstellar time-scales at grain temperatures up to the sublimation temperature of ice at 90–100 K. Since the proposed hop-and-turn mechanism depends on the existence of point defects present in the ice and on the defect concentrations, the study was extended to amorphous water samples by Fisher & Devlin (1995). Indeed, they found a much lower activation energy of the turn step involved, ∼3000 K. Studies of exchange on ice surfaces – also subject to larger structural defects – indicated an enhanced L-defect activity (Uras-Aytemiz et al. 2001). These studies were performed, however, using ices doped with HCl in order to have a higher sensitivity. Protons are generated via the reaction $HCl + H_2O \rightarrow H_3O^+ + Cl^-$, the exothermicity of which could influence the local processes that occur (Kim, Kim & Kang 2009). Doping creates additional (shallow) proton traps in the ice in the vicinity of the counterion (Uras-Aytemiz et al. 2001), and proton films can remain inactive up to around 125 K (Lee et al. 2007), both of which can influence the reaction rates detected. Moon et al. (2010) showed that doping lowers the activation energy found for H/D exchange on surfaces by almost a factor of 2.

A similar situation applies to space. In the ISM ices do not have a perfectly ordered structure, partially because they are (i) not condensed at high enough temperatures, (ii) comprised of many species that are formed on the surface, (iii) composed of more molecules than only water, and (iv) subject to structural changes upon energetic processing of the ice. These effects will contribute to a high defect concentration in interstellar ices.

In this paper, we aim to bring together the previous results of these scientific communities – physical chemistry, cometary chemistry and (laboratory) astrochemistry – while presenting several new experimental results of which the relevance to astronomy is discussed. We discuss amorphous D_2O:H_2O ices with mixing ratios around 1:1. Although such ratios are not astrochemically relevant, they do allow for a higher sensitivity of the proton exchange process at lower temperatures, without the necessity to use doping. We mimic the high expected amount of defects in the ISM by intentionally growing amorphous ice structures at temperatures of 15 K and probe whether this higher defect concentration in the ice structure, see Fig. 1, leads to an increase of the reaction rate for reaction R1. The results are extended to a more general concept taking into account 'all' hydrogen-bonded molecules. Subsequently, the

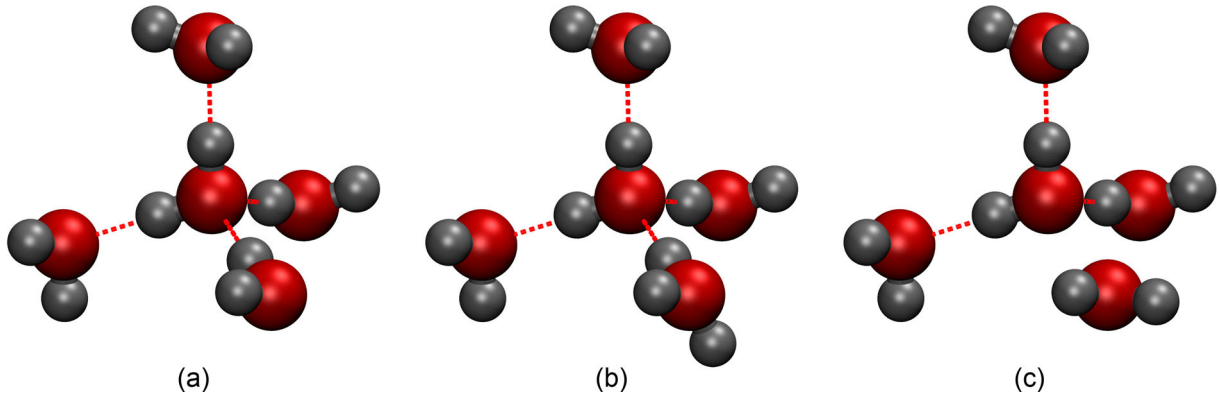

Figure 1. (a) Water molecule surrounded by four hydrogen-bonded molecules as in an ideal crystal structure, (b) water molecule surrounded by four hydrogen-bonded water molecules, where one of those contains an extra proton: ionic defect, and (c) water molecule surrounded by four water molecules, with one of those rotated causing a missing hydrogen bond: 'L-defect'.

astrochemical implications are discussed focusing on the relevance of proton/deuteron swapping at long time-scales, but at temperatures below full ice desorption.

2 METHODS

All experiments studied here consist of two sequential steps: (a) the simultaneous deposition of H_2O (Milli-Q) and D_2O (Sigma-Aldrich 99.96 per cent) on the substrate at 15 K and subsequently; (b) an isothermal experiment at a given temperature ($T_{iso} \geq 90$ K) during which the level of proton exchange is probed by means of reflection absorption infrared spectroscopy (RAIRS). In one experiment (Section 3.2) also a quadrupole mass spectrometer (QMS) is used. Below, the experimental procedure is described first, followed by an explanation of the calibration experiments performed, the analysis of the spectra, and the analysis of the temporal evolution of the surface abundances of H_2O, HDO, and D_2O.

2.1 Experimental

Experiments are performed using the SURFace REaction SImulation DEvice (SURFRESIDE$_2$) setup, which has been constructed to systematically investigate solid-state reactions leading to the formation of molecules of astrophysical interest at cryogenic temperatures. The setup has been extensively described in Ioppolo et al. (2013) and therefore only a brief description of the procedure is given here. All performed experiments and the corresponding molecular deposition rates are listed in Table 1. The results of experiments 1–10 are discussed in Section 3.1. Experiment 11 follows a procedure similar to that for the water experiments described below and is discussed in Section 3.2. The method used for experiment 12 deviates and is discussed in Section 3.2.

SURFRESIDE^2 consists of three ultrahigh vacuum (UHV) chambers: one main chamber for ice growth, ice processing, and ice diagnostics, and two chambers comprising atom beam lines. All have a room-temperature base-pressure between 10^{-9} and 10^{-10} mbar. A rotatable gold-coated copper substrate in the centre of the main chamber is cooled to the desired temperature using a He closed-cycle cryostat with an absolute temperature accuracy of $\leq$2 K. Both water and heavy water are prepared in a separate pre-pumped ($\leq 10^{-5}$ mbar) dosing line and after several freeze-pump-thaw cycles a co-deposition of room-temperature vapour H_2O and D_2O is performed. One species is deposited through a metal deposition line under an angle of 90° and the other through one of the separate UHV beam lines at an angle of 135° with respect to the plane of the surface, see Table 1. This UHV beam line can be operated independently and can be separated from the main chamber by a metal shutter. Deposition takes place at a surface temperature of 15 K to ensure a large amount of amorphicity of the ice (see discussion above).

After approximately 60 min of co-deposition at low temperature, yielding 45–65 ML, the substrate is heated up to the desired temperature, T_{iso}, between 90 and 140 K. Note that in the laboratory ices sublimate not at 100 K, but rather between 145 and 165 K, hence the higher temperatures employed here. The warm-up phase clearly

Table 1. List of (calibration) experiments and corresponding parameters; temperature (T), beamline angle to the plane of the surface, and molecular flux (f).

	Experiments					
	T_{iso} (K)	90°	f_{dep} (cm^2 s^{-1})	135°	f_{dep} (cm^2 s^{-1})	t_{iso} (min)
1	90	D_2O	10 $^{(12)}$	H_2O	10 $^{(12)}$	270
2	100	D_2O	10 $^{(12)}$	H_2O	10 $^{(12)}$	270
3	120	D_2O	10 $^{(12)}$	H_2O	10 $^{(12)}$	360
4	125	D_2O	10 $^{(12)}$	H_2O	10 $^{(12)}$	270
5	130	D_2O	10 $^{(12)}$	H_2O	10 $^{(12)}$	210
6	130	D_2O	4 $^{(12)}$	H_2O	10 $^{(12)}$	190
7	135	D_2O	10 $^{(12)}$	H_2O	10 $^{(12)}$	150
8	140	D_2O	10 $^{(12)}$	H_2O	10 $^{(12)}$	110
9	140	D_2O	4 $^{(12)}$	H_2O	10 $^{(12)}$	120
10	140	H_2O	4 $^{(12)}$	D_2O	10 $^{(12)}$	120
11	130	D_2O	10 $^{(12)}$	NH_3	7 $^{(12)}$	120
12[a]	TPD	D_2O	–	NO + H	–	–
	Calibration experiments					
1	var.[b]	H_2O	20 $^{(12)}$	–	–	–
2	var.[b]	HDO	10 $^{(12)c}$	–	–	–
3	var.[b]	D_2O	19 $^{(12)d}$	–	–	–
4	var.[b]	–	–	–	–	–

Note. The notation α $^{(\beta)}$ implies $\alpha \times 10^{\beta}$.
[a]Instead of a full co-deposition, a layered experiment was performed, first co-depositing NO + H to prepare a NH_2OH layer, which was then covered by D_2O. [b]Spectra were acquired at all temperatures relevant for the experiments, i.e. 90–140 K. [c]Due to the mixture preparation of HDO, the statistical ratio between the constituents H_2O:HDO:D_2O is 1:2:1. [d]The effective deposition rate is somewhat lower as a result of HDO contamination in the D_2O sample, this is estimated to be $\leq$5 per cent from the OH stretching mode.

affects the porosity of the ice (Bossa et al. 2012) and therefore also the ice structure. However, using H_2O:D_2O mixing ratios around 1:1, each molecule initially has at least one neighbour of its isotopic counterpart, which renders the degree of porosity less important. Note also that the extra collapse of the pores at 120 K with respect to that at 90 K is only 3 per cent (Bossa et al. 2012). Thus, assuming locally distorted hydrogen-bonded structures (Karssemeijer et al. 2014, Karssemeijer, personal communication)[1], the exact structure of the ice and/or diffusion mechanisms (Jung et al. 2004; Oxley, Zahn & Pursell 2006) do not play a role here. A RAIR difference spectrum with respect to the background is acquired every 5 or 10 min up to the final time of the experiments, t_{iso} in Table 1. The background spectrum is acquired from an empty surface prior to the co-deposition at low temperature. RAIR spectra comprise a spectral range between 4000 and 700 cm^{-1} with a spectral resolution of 1 cm^{-1} and are averaged over 512 scans. Exchange occurs faster at higher temperatures, therefore those experiments have a shorter duration. Pure component calibration spectra are used for the analysis of the experiments, see Section 2.2.

The deposition rates mentioned in Table 1 are calculated using the following relation:

$$\frac{c_{X_2O}\ P_{X_2O}\ \langle v \rangle}{4\ k_B\ T}, \quad (1)$$

where c_{X_2O} is the calibration factor for the pressure gauge for the three isotopologues of water (X_2O = H_2O, HDO, or D_2O), v is the thermal velocity of the vapour molecules at 300 K, k_B is the Boltzmann constant, and T corresponds to the (room) temperature. The calibration factor for water is 1/0.9. There is no significant difference found between the absolute partial cross-sections for electron-impact ionization of H_2O and D_2O, which could in principle influence the pressure reading of the gauge (Straub et al. 1998; Itikawa & Mason 2005). Therefore, we assume that this is also the case for HDO and all calibration factors for the pressure are taken to be equal.

Note that the initial spectra of experiments 1–5, 7 and 8 at 15 K after deposition are compared with each other to confirm the reproducibility: each low-temperature spectrum is analysed with the fitting procedure described below and the initial surface abundances of water and deuterated water are found to be reproducible with a standard deviation of ∼5 per cent.

2.2 Spectral fitting

Each spectrum is the sum of the pure H_2O, HDO, and D_2O components along with their intermolecular interactions. The intermolecular interactions cannot be captured in pure calibration spectra and they are stronger in the IR stretching than bending region. Furthermore, the bending region is less sensitive to crystallization effects. Therefore, our region of interest lies in the 2000–1000 cm^{-1} range, where the H_2O, HDO, and D_2O molecules vibrate in their respective bending modes: 1660, 1490, 1250 cm^{-1}. Upon proton/deuteron exchange the H_2O and D_2O intensities decrease, whereas the HDO intensity increases.

The integrated area of each mode can be converted into a number of molecules, assuming that band strengths are available, but in reflection mode these are typically ill-constrained. To be able to quantify the dynamics at work, a spectral fitting procedure is needed to separate the three components. For this purpose, also three calibration experiments are performed.

[1] Based on the ASW samples used in Karssemeijer et al. (2014).

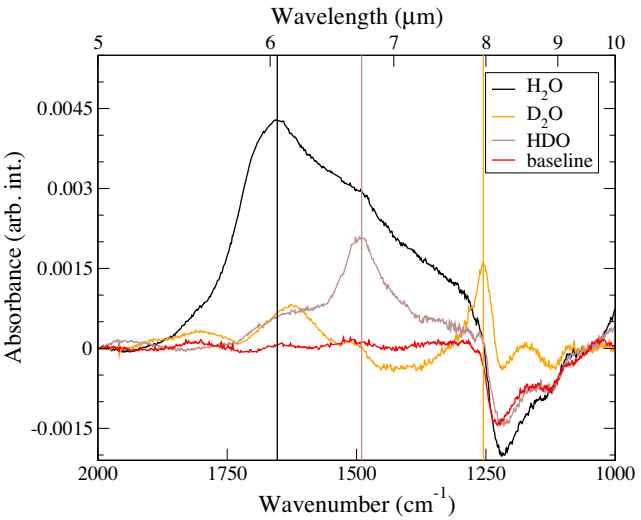

Figure 2. Bending region of the calibration spectra used for fitting the experiments, all spectra are recorded at 130 K. See text concerning the 1625 cm^{-1} band in the D_2O spectrum, the contamination in the HDO band, and the baseline artefact around 1200 cm^{-1}.

A calibration experiment, see final rows of Table 1, consists of the deposition of a 'pure' X_2O component for 30 min at 15 K and spectrum acquisition thereafter at all temperatures relevant for the experiments performed, i.e. 90, 100, 120, 125, 130, 135, and 140 K. At each temperature, the spectrum looks slightly different and therefore pure spectra for each temperature are necessary for the fitting procedure. Furthermore, in the spectral region between ∼1050 and ∼1250 cm^{-1} a known temperature-dependent artefact is present, which makes it necessary to record blank spectra at all relevant temperatures as well. It is most likely due to a temperature dependence in the absorption of our background sample. These spectra are also included in the fits (calibration experiment 4), but do not fully correct for the effect, as explained below.

Using the pure components, we avoid having to correct for the difference in band strengths: each pure spectrum consists of a known amount of deposited H_2O, HDO, and D_2O. A second band around 1625 cm^{-1} in the D_2O spectrum has its origin in the combination mode $\nu_{bending} + \nu_{libration}$ (Bertie & Whalley 1964). There is also a small OH stretching signal present in the spectrum, but it is ≤5 per cent with respect to the OD stretching signal. HDO was prepared by mixing equal amounts of H_2O and D_2O vapours into a pre-pumped ($\leq 10^{-5}$ mbar) dosing line. We expect the hydrogen and deuterium atoms to be distributed statistically, resulting in a statistical 1:2:1 mixture. That means that the effective HDO deposition rate is only half of the total deposition rate for this particular experiment. The spectra shown in Fig. 2 are used for the fitting procedure. The HDO spectrum cannot be obtained pure, due to the way it is produced in the dosing line. In the fitting procedure, we used both the original spectrum as well as a spectrum corrected for the H_2O and D_2O contamination in the HDO contribution, see Section 2.4.

Every separate experiment is composed of a time-resolved series of recorded spectra, each providing a snapshot of the ongoing proton exchange process. A non-negative least-squares solver is used to fit the pure components to the spectrum only in the bending range of 2000–1000 cm^{-1}. Fig. 3 depicts an example of such a fit for the final spectrum (recorded after 210 min) recorded during experiment 5 from Table 1. In this case, the baseline does not contribute to

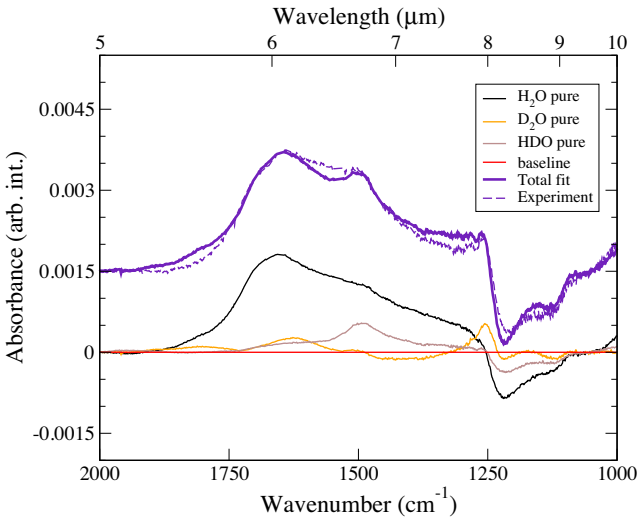

Figure 3. Example of a recorded spectrum in the water bending region (130 K) and its best fit, decomposed into the separate components (H_2O, HDO, and D_2O – see Fig. 2), recorded after 210 min. Note: this concerns experiment 5 from Table 1. Pure spectra themselves compensate for the baseline artefact at 1200 cm^{-1}.

the fit since the sum of the pure components themselves already compensate for the artefact. Usually, however, the temperature-dependent baseline is needed to take care of this artefact.

2.3 Reaction dynamics

The total contribution of each pure component to the fit is subsequently plotted versus time in order to resolve the dynamics. We are not able to observe the isolated HDO entities in a water matrix that have been proposed to be produced through a hop-and-turn mechanism (Collier et al. 1984), because both reaction partners are present in the ice with mixing ratios between 1:2 and 2:1. Because of this, our system is intrinsically easier to model, since we observe only the proton or deuteron hopping, leading to a reaction system of the forward and backward reactions, R1 with rate k_f and R2 with rate k_r. They can be evaluated in terms of a mean field approximation. The temporal evolutions of the concentrations (or abundances) can be described with a set of ordinary differential (rate) equations:

$$\frac{\mathrm{d[H_2O]}}{\mathrm{dt}} = -k_f[\mathrm{H_2O}][\mathrm{D_2O}] + k_r[\mathrm{HDO}]^2 \quad (2)$$

$$\frac{\mathrm{d[D_2O]}}{\mathrm{dt}} = -k_f[\mathrm{H_2O}][\mathrm{D_2O}] + k_r[\mathrm{HDO}]^2 \quad (3)$$

$$\frac{\mathrm{d[HDO]}}{\mathrm{dt}} = 2\,k_f[\mathrm{H_2O}][\mathrm{D_2O}] - 2\,k_r[\mathrm{HDO}]^2\,, \quad (4)$$

where $\frac{\mathrm{d[H_2O]}}{\mathrm{dt}} + \frac{\mathrm{d[D_2O]}}{\mathrm{dt}} + \frac{\mathrm{d[HDO]}}{\mathrm{dt}} = 0$. We assume thermal desorption to be negligible at these temperatures. Using an optimization algorithm in conjunction with a least-square ODE solver, k_f and k_r can be extracted for each experiment. $[H_2O]_0$, $[HDO]_0$, and $[D_2O]_0$ are taken equal to the values found for each experiment. Section 2.4 discusses several examples of both the temporal evolution of the pure components as well as the modelled result via the rate equations. Note that the start of each experiment is almost exclusively sensitive to k_f, since $[HDO]_0$ is always low. We therefore chose to use the first 33 per cent in time, while still in the linear regime, of the experiment to determine k_f. A discussion on this topic is given in the section below.

2.4 Optimization procedure

Fig. 4 depicts three examples of our modelled results, for temperatures of 90, 125, and 140 K (experiments 1, 4, and 8 in Table 1). The top row, panels (a)–(c), shows the HDO fit to the experiments for the first 33 per cent of the experiment, and from the (near-) linearity of the experimental slopes it can be deduced that it is indeed sensitive mainly to k_f. In panels (d)–(f), the time evolution of the experimental and modelled abundances (equations 2–4) for all three species is plotted for the entire experimental time.

Analysing the abundances at 90 K, we find an apparent discrepancy for the temporal evolution of D_2O. While the recorded H_2O and HDO abundances remain constant in time, since there is no proton exchange at this low temperature, the D_2O abundance does not. Inspection of the IR spectra shows that this is likely caused by the spectroscopic artefact between ∼1050 and ∼1250 cm^{-1} mentioned above. This artefact actually partially overlaps with the D_2O signal. We therefore decided not to include the heavy water abundance explicitly in the determination of the optimal reaction rates, but to check in retrospect whether or not the modelled abundance is in approximate agreement with the experiments.

Furthermore, the graphs at high temperature (140 K) show that both modelled H_2O and D_2O abundances deviate somewhat from the experiment. To further constrain this, we have studied two limiting cases of the dependence of the H_2O and D_2O abundances on the HDO calibration spectrum: (a) assuming a 'pure' HDO calibration spectrum and (b) assuming a statistical 1:2:1 distribution between H_2O:HDO:D_2O for the deposited HDO. Unfortunately, the HDO ice which we deposited to obtain our HDO calibration spectrum did not only contain HDO, but also H_2O and D_2O. If we do not account for this in our calibration spectrum (case a), the water and heavy water contribution are underestimated during the fitting procedure. Accounting for the presence of both contaminants in the HDO calibration spectrum by assuming a statistical distribution (case b) will on the contrary lead to an overestimation of the H_2O and D_2O abundances. Therefore, we decided to optimize the model and obtain k_f and k_r by using only the HDO abundance. Subsequently, we verified that the modelled water and heavy water abundances fall within the range determined by the two limiting cases for the obtained values of k_f and k_r.

Thus, the optimization sequence used for modelling the HDO abundance is as follows:

(i) k_f is optimized by modelling the first 33 per cent in time of the experiment with $k_r = 0$;

(ii) k_r is optimized by modelling the final 33 per cent in time of the experiment with k_f fixed to the value found in (i);

(iii) k_f is optimized again by modelling the full experiment with k_r fixed to the value found in (ii).

The error function used for this optimization is

$$E_{\mathrm{HDO}} = \sum_{t_1}^{t_2} \frac{1}{\Delta t} \frac{\left([\mathrm{HDO}]_{\mathrm{model}}(t) - [\mathrm{HDO}]_{\mathrm{exp}}(t)\right)^2}{\left\langle [\mathrm{HDO}]_{\mathrm{model}}(t) + [\mathrm{HDO}]_{\mathrm{exp}}(t) \right\rangle}\,. \quad (5)$$

The reaction rates leading to the lowest error are selected to be used in next iterations or are stored as the optimum rates.

Finally, the activation energy of R1 is determined by an Arrhenius fit of the different reaction rates versus temperature. The error associated with this fit is determined with the stats subpackage of SCIPY in PYTHON and corresponds to the standard error of the slope.

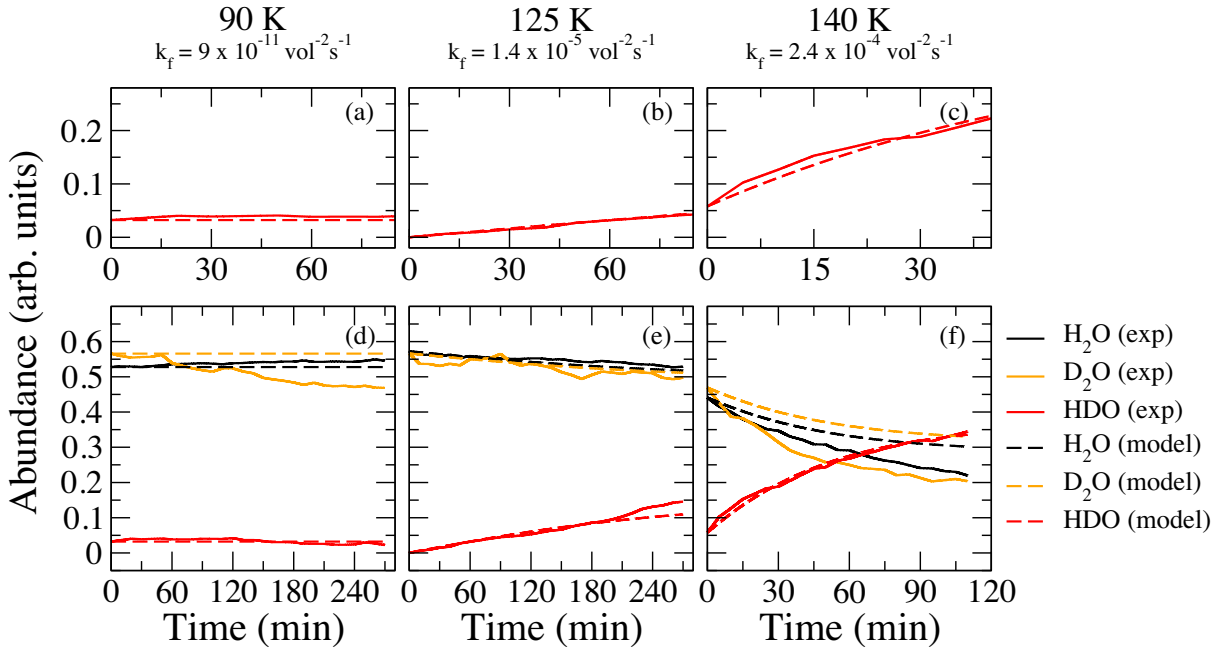

Figure 4. Modelled H_2O, D_2O, and HDO concentrations for experiments 1 (a and d), 4 (b and e), and 8 (c and f) (Table 1). The top row, panels (a)–(c), are zoom-ins of the HDO experimental and modelled abundance for the first 33 per cent of the experimental duration. The bottom row, panels (d)–(f), depicts the evolution of all three components for the entire duration.

3 RESULTS AND DISCUSSION

3.1 Activation energy of proton exchange in H_2O:D_2O mixtures

The reaction rates obtained from the reaction dynamical fitting by a simple rate equation model are converted into an activation energy with the use of an Arrhenius expression:

$$k = \nu \exp\left(\frac{-E_a}{k_B T}\right). \quad (6)$$

In this expression the prefactor, ν, represents a trial frequency related to the vibrations of a species in a local potential well and corresponds to values between 10^{12} and 10^{13} s^{-1} (Hasegawa, Herbst & Leung 1992). Fig. 5 depicts $\ln(k_f)$ versus $1/T$. If experiments 2–10 are included in the determination of the activation energy, a value of 3840 ± 125 K is found. The error given here is the error of the slope. The exact value found for the activation energy changes when the amount of assumed contamination in the HDO spectrum is varied, i.e. going from case (a) to (b). The resulting values, however, are not significantly different as assessed by a two-sided student's *t*-test ($p < 0.05$).

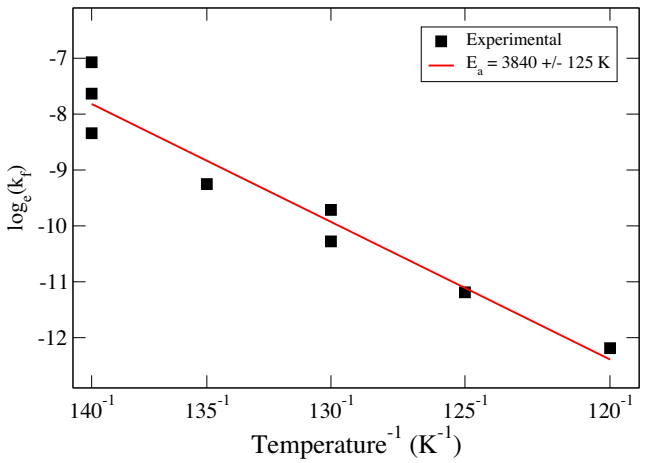

Figure 5. Arrhenius plot for k_f.

As stated before, Wooldridge & Devlin (1988) found a substantially higher activation energy of ∼5000 K associated with reaction R1. They proposed a mechanism of proton transfer that occurs via ionic defects in the ice. These defects will be more prominent in an amorphous ice and indeed the rate increases drastically; $e^{-3840/T}/e^{-5000/T} > 4000$ for $T \leq 140$ K. The specific implications of this for astrochemical environments are discussed in Section 5.

Experiments below 130 K are not sensitive to k_r, because the situation in which enough HDO molecules are next to each other is never reached within the experimental duration. For our experiments at 130–140 K, it is not possible to find any correlation between k_r and the temperature, again because for the largest part of the experiment there are not enough HDO molecules close to each other. However, Collier et al. (1984) suggested that $k_r < k_f$ in the case of an isolated D_2O molecule in an H_2O surrounding, as a result of the local structure. This can also be explained from a more theoretical free energy point of view. The total Gibbs free energy of the reaction, G, is determined by the enthalpies, H, and entropies, S, of the molecules:

$$\Delta G(2\,\text{HDO-H}_2\text{O-D}_2\text{O}) = \Delta H_f - \text{T} \cdot \Delta S_f\,. \quad (7)$$

Using the gas-phase data reviewed in Chase (1998), this leads to the following expression:

$$\Delta G = 290 - T \cdot 11.86 \quad \text{J mol}^{-1} \quad (8)$$

$$= 34.88 - T \cdot 1.43 \quad \text{K}\,. \quad (9)$$

Although the thermochemistry in the solid state is affected by the local structure, the gas-phase expression given above does show that the driving force is the entropy change and that the reaction becomes clearly exergonic at higher temperatures only, hence we also expect that $k_r < k_f$. If this relation is incorporated into the optimization procedure, the activation energy found does not differ significantly from 3840 K.

Finally, note that here no conclusions can be drawn concerning the prefactor ν, because accurate values for the band strengths are lacking.

3.2 Proton exchange in other hydrogen-bonded molecules

As mentioned in the Introduction, proton exchange in ices has been studied previously for several (mixtures of) hydrogen-bonded molecules. Here, we mention these studies specifically and extend the studies of water to a more general ice theme: proton exchange in hydrogen-bonded molecules. As long as so-called proton wires exist between the hydrogen-bonded molecules, exchange is expected to be rapid (Bertie & Devlin 1983). A proton wire can be thought of as a chain of hydrogen-bonded molecules that has the flexibility to transfer protons from one to the next molecule. In such a way, any ionic defect in the ice can be easily passed on to the neighbouring molecule and hence protons and deuterons can move efficiently. The following ice mixtures are briefly discussed: NH_3:D_2O, CD_3OD:H_2O, CD_3ND_2:H_2O, and NH_2OH:D_2O.

Exchange between isolated NH_3 in an amorphous D_2O ice was found to be faster than in pure water ice and much faster than for crystalline ammonia (Thornton et al. 1981; Bertie & Devlin 1983). We have performed a similar experiment, co-depositing NH_3 and D_2O (2:3) at low temperature and heating to 130 K, experiment 11 in Table 1. Indeed rapid exchange of protons can be confirmed. A steady-state HDO concentration is reached at least three times faster than in the case of water (experiment 5). This shows once more that amorphicity can enhance the exchange rates.

Concerning the case of isolated amorphous d4-methanol mixed with water, both Ratajczak et al. (2009) and Souda et al. (2003) confirmed thermal exchange to be efficient at laboratory time-scales starting from 120 K. Note that this exchange concerns specifically the hydroxyl group of methanol. The C–D (or C–H) bonds do not participate in any hydrogen bonding network and are therefore not exchanged via this mechanism. They can, however, be exchanged via deuterium bombardment of CH_3OH as discussed by Nagaoka, Watanabe & Kouchi (2005).

Ratajczak (2012) also studied the exchange of isolated methylamine (CD_3ND_2) with water and found similar results as for methanol: exchange takes place only on the amine entity of the molecule and is detectable from 110 K onwards.

Here, in light of recent studies highlighting the hydrogenation of NO molecules and the subsequent formation of NH_2OH (Congiu et al. 2012; Fedoseev et al. 2012), we also performed an experiment probing the exchange between D_2O and NH_2OH (experiment 12, Table 1). In this case, both hydrogen bearing groups are able to form hydrogen bonds. A layer of NH_2OH is grown following a similar procedure as described by Fedoseev et al. (2012) and capped with a layer of D_2O at 15 K. Increasing the sample temperature to 130 or 140 K could lead to exchange of protons and deuterons on the interface of the two molecular layers. However, proton exchange is not clearly visible by RAIR spectroscopy due to overlapping band frequencies between the NH(D) and OD(H) groups. Therefore, a temperature programmed desorption experiment is performed, during which the molecules gain more mobility increasing the probability that NH_2OH and D_2O meet, albeit for a short time until full desorption takes place. This experiment resulted in the detection of mass to charge ratios of 19, 34, 35, and 36 in the QMS, see Fig 6. In this figure, the intensity does not reflect the *in situ* IR intensity, but the intensity of gas-phase species after evaporation from the surface during a linear heating of the substrate. The temperature indicates the surface temperature at which this evaporation occurs. These masses correspond to the molecules HDO, singly and doubly deuterated NH_2OH, and ND_2OD. This confirms proton exchange in the amine and hydroxyl groups, both of which have hydrogen bonds.

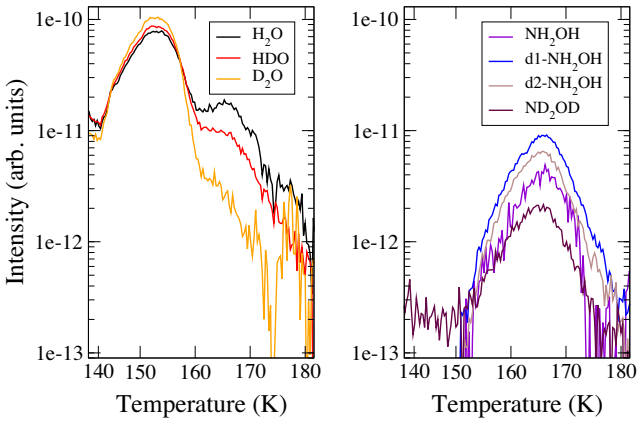

Figure 6. QMS traces for TPD experiments of mass to charge ratios of 18, 19, 20, 33, 34, 35, and 36 probing exchange in a layered NH_2OH:D_2O ice. Note that the *x*-axis changed to temperature.

4 EXPERIMENTAL CONCLUSIONS

The thermal process of proton/deuteron exchange between water and its isotopologues has been studied in mixed ices. Using RAIR spectra, the time evolution of the characteristic vibrational bending modes of H_2O, HDO, and D_2O has been monitored as a function of temperature. In particular, H_2O and D_2O have been grown at 15 K and heated up to a desired temperature where the occurrence of HDO has been probed indicating that the reaction $H_2O + D_2O \rightarrow 2$ HDO takes place. Temperatures between 90 and 140 K have been considered and a reaction rate for each temperature has been determined with the use of a simple rate equation model. The linearity of the resulting Arrhenius plot in Fig. 5 shows that it is reasonable to express the rate through thermal activation and an activation energy of 3840 K has been found.

Ratajczak (2012) suggests that proton exchange coincides with crystallization. However, exchange has been found to take place prior and post crystallization, both in the work presented here as well as by Wooldridge & Devlin (1988), Fisher & Devlin (1995), and Gálvez et al. (2011). In the ISM, (F)UV radiation would render the ices largely compact amorphous by destruction of local molecules and recombination of its fragments. Exothermic energy release upon molecule formation is likely to have the same effect (Palumbo 2006; Oba et al. 2009).

In this study, we mimic the lack of long-range order in interstellar ices by intentionally growing amorphous ice structures. The aim is to investigate whether a higher concentration of structural defects (see Fig. 1) in amorphous ices with respect to crystalline structures leads to exchange rates high enough to become relevant on interstellar time-scales. We indeed find a lower overall (or rate-determining) activation energy associated with the exchange in

Table 2. Typical thermal exchange time-scales at various grain temperatures and activation energies.

T (K)	$E_a = 5000$ K[(a)]	$E_a = 3840$ K[(b)]
70	3.3×10^{11} yr	2.1×10^{4} yr
80	4.4×10^{7} yr	2.2×10^{1} yr
90	4.2×10^{4} yr	1.1×10^{-1} yr

Notes. [(a)] Wooldridge & Devlin (1988). [(b)]This work

non-doped amorphous ices with non-energetic detection methods compared to crystalline ices: 3840 versus 5000 K. This corresponds to the quantitative findings of Fisher & Devlin (1995) for doped ices, those of Moon et al. (2010) for pure ice surfaces and to the qualitative results mentioned by Gálvez et al. (2011). The latter paper also discusses H/D exchange in water ices, but from the point of view to investigate whether HDO detections in ice are possible.

Assuming a value of 10^{12} s^{-1} for the prefactor ν in equation (6), this corresponds to typical time-scales as summarized in Table 2. The large differences covering orders of magnitude of the typical time-scales of proton exchange clearly show the importance of incorporating the correct activation energy.

5 ASTROCHEMICAL IMPLICATIONS

Interstellar ices are likely to be defect-rich by nature because of the many ice components and various types of (energetic) processing. Furthermore, since ices consist mainly of water, the hop-and-turn mechanism is likely to dominate proton exchange, while, simultaneously, the existence of the proton wires mentioned above is key to efficient transfer.

5.1 Protostellar and protoplanetary environments

The typical time-scales derived with the experimentally found activation energy can be compared to interstellar time-scales, i.e. those mentioned in Table 2 and those obtained for protostellar and protoplanetary disc environments. Schöier et al. (2002) showed that the transit time for grains and molecules through the warm, dense region around the hot core IRAS 16293−2422 is of the order of several hundred years. Ices present at temperatures above 80 K can thus be influenced by scrambling. Furthermore, although the high dust-temperature regions in discs concern only the inner few mid-plane AU (Walsh, Millar & Nomura 2010), turbulent vertical and radial mixing can result in transportation of water from the mid-plane to disc surface (Furuya et al. 2013; Albertsson, Semenov & Henning 2014). This is part of a cycle in which atomic oxygen is transported to the mid-plane and reforms water and/or other molecules. Since the grains are transported, also the time they pass at higher temperatures is longer, hence allowing proton scrambling to take place. This then applies to all hydrogen-bonded molecules. Mixing time-scales are determined by the ratio between the column density of water and the flux in upward or radial direction (Furuya et al. 2013). They find that typical time-scales range between 10^4 and 10^7 yr for radii between 1 and 200 AU and that the radial accretion time-scale is of a similar order of magnitude and are long enough to allow scrambling to take place.

Comparing typical dynamical time-scales in protostellar and protoplanetary disc environments to the values listed in Table 2, we find that an activation energy of 3840 K renders the thermally activated H/D exchange relevant at static dust temperatures of 70 K and above.

We would therefore expect a D_2O detection probability lower than determined statistically in high-temperature regions, because any D_2O available in the ice is likely to be converted into two HDO molecules given enough time.

In fact, consistent with this conclusion, in the warmer regions surrounding NGC 1333 IRAS2A Coutens et al. (2014) found a lower D_2O/HDO ratio than in the cold envelope layer around IRAS 16293−2422 (Coutens et al. 2013). The higher D_2O/HDO than HDO/H_2O ratios reported in both cases are currently under debate. Two possible causes are that either (i) the surface deuteration chemistry network is ill-constrained or (ii) that both sublimation of grain mantles and water formation at higher gas-phase temperatures takes place in the inner regions of this source. Alternatively, if high D_2O abundances compared to modelled results turn out to be common (Coutens et al. 2013, 2014), it must be because the ice mantle does not encounter high temperatures for long enough times. This means that the time-scales derived here can also be used in the opposite way, to determine an upper limit for the time that an icy grain resides in an area of a certain temperature. Currently, the limited number of observations does not allow us to draw such a conclusion.

5.2 Cometary ices

Shifting focus towards the application of exchange in cometary ices, we note that to the best of our knowledge no large ice chemistry models of comets exist. In the gas-phase coma model of Rodgers & Charnley (2002), a high ice abundance is sublimated as a given initial condition. The ice itself, however, is not modelled. They found that the D/H ratio in gas-phase coma species is determined by the ratio in their parents. Thus, the ice in fact does determine the deuterium fractionation found in the coma. Ideally, ice abundances should be determined by a cometary ice chemistry model incorporating low- and high-temperature chemistry, as well as sublimation effects to investigate the effect of accumulative heating on ices.

Thermal chemistry, in particular H/D transfer, can play a major role in the thick cometary ices, changing the deuterium fractionation of many species, because HDO is the main deuterated component of these ices.

The recent results on the HDO/H_2O ratio in the coma of comet 67P/Churyumov–Gerasimenko and the discrepancy with respect to the D/H ratios in other Jupiter family comets shows that it is crucial to understand the effect of thermal processing of ice constituents (Altwegg et al. 2015).

5.3 Proof-of-principle modelling

Scrambling of deuterons at high temperatures can alter the D/H ratios and therefore should be taken into account, when using D/H ratios to determine the cosmic origin of the water on Earth. This holds not only for the main component of interstellar ice, water, but especially also for any species that has an N–H or O–H bond that can participate in hydrogen bonding. Molecules detected in the ISM with such functional groups, most of which are thought to have been formed on the surface of dust grains, are e.g. HNO, HNC, HNCO, HNCS, NH_3, NH_2OH, CH_3OH, $HCONH_2$, CH_3NH_2, NH_2CH_2CN, CH_3CH_2OH, $(CH_2OH)_2$.

In all examples mentioned in Section 3.2 the hydrogen-bonded network for OH and NH moieties plays a crucial role in H/D

exchange. Moreover, functional groups with CH that do not participate in hydrogen bonds do not exchange their proton thermally.

We emphasize that as a first approximation exchange of protons and deuterons between water and other hydrogen-bonded species should be modelled using an activation energy of ∼3840 K both in disc structures as well as in cometary ices.

Note that as discussed above, the forward and backward reaction rates are not expected to be equal, due to a more favourable entropy for the reaction $H_2O + D_2O \rightarrow 2\,HDO$ with respect to the backward reaction. Although the activation energy itself is constrained only for the case of water and its deuterated analogues, arguments of enthalpy and entropy can also aid in constraining the reaction rates of H/D transfer for other molecules, as suggested by our experiments listed in Table 1. Finally, reactions with no net effect, such as $H_2O + HDO \rightarrow HDO + H_2O$, only have meaning in a microscopic model, where they can be seen as analogues of diffusion. Thus, in a rate equation based model, they can be omitted.

ACKNOWLEDGEMENTS

We thank Fabrizio Puletti and Ko-Ju Chuang for their help in the laboratory, Leendertjan Karssemeijer for his help with the hydrogen-bonded water structures, and Ewine van Dishoeck, Xander Tielens, Magnus Persson, and François Dulieu for stimulating discussions.

Astrochemistry in Leiden is supported by the European Community's Seventh Framework Programme (FP7/2007- 2013) under grant agreement no. 238258, the Netherlands Research School for Astronomy (NOVA) and from the Netherlands Organization for Scientific Research (NWO) through a VICI grant. TL is supported by the Dutch Astrochemistry Network financed by The Netherlands Organization for Scientific Research (NWO). Support for SI from the Marie Curie Fellowship (FP7-PEOPLE-2011-IOF-300957) is gratefully acknowledged. HMC is grateful for support from the VIDI research program 700.10.427, which is financed by The Netherlands Organization for Scientific Research (NWO) and from the European Research Council (ERC-2010-StG, grant agreement no. 259510-KISMOL).

REFERENCES

Aikawa Y., van Zadelhoff G. J., van Dishoeck E. F., Herbst E., 2002, A&A, 386, 622
Albertsson T., Semenov D., Henning T., 2014, ApJ, 784, 39
Altwegg K. et al., 2015, Science, 347, 27
Bergin E. A., Tafalla M., 2007, ARA&A, 45, 339
Bertie J. E., Devlin J. P., 1983, J. Chem. Phys., 78, 6203
Bertie J. E., Whalley E., 1964, J. Chem. Phys., 40, 1637
Bockelée-Morvan D. et al., 2000, A&A, 353, 1101
Bossa J.-B., Isokoski K., de Valois M. S., Linnartz H., 2012, A&A, 545, A82
Butner H. M., Charnley S. B., Ceccarelli C., Rodgers S. D., Pardo J. R., Parise B., Cernicharo J., Davis G. R., 2007, ApJ, 659, L137
Caselli P., Ceccarelli C., 2012, A&AR, 20, 56
Chase M. W., 1998, Journal of Physical and Chemical Reference Data, Monograph, no. 9. Am. Chem. Soc., Washington, DC
Cleeves L. I., Bergin E. A., Alexander C. M. O., Du F., Graninger D., øberg K. I., Harries T. J., 2014, Science, 345, 1590
Collier W. B., Ritzhaupt G., Devlin J. P., 1984, J. Phys. Chem., 88, 363
Congiu E. et al., 2012, ApJ, 750, L12
Coutens A. et al., 2013, A&A, 553, A75
Coutens A., Jørgensen J. K., Persson M. V., van Dishoeck E. F., Vastel C., Taquet V., 2014, ApJ, 792, L5
Fedoseev G., Ioppolo S., Lamberts T., Zhen J. F., Cuppen H. M., Linnartz H., 2012, J. Chem. Phys., 137, 054714
Fisher M., Devlin P., 1995, J. Phys. Chem., 99, 11584
Fuchs G. W., Cuppen H. M., Ioppolo S., Romanzin C., Bisschop S. E., Andersson S., van Dishoeck E. F., Linnartz H., 2009, A&A, 505, 629
Furuya K., Aikawa Y., Nomura H., Hersant F., Wakelam V., 2013, ApJ, 779, 11
Gálvez Ó., Maté B., Herrero V. J., Escribano R., 2011, ApJ, 738, 133
Grim R. J. A., Greenberg J. M., de Groot M. S., Baas F., Schutte W. A., Schmitt B., 1989, A&AS, 78, 161
Hasegawa T. I., Herbst E., Leung C. M., 1992, ApJS, 82, 167
Hiraoka K., Miyagoshi T., Takayama T., Yamamoto K., Kihara Y., 1998, ApJ, 498, 710
Ioppolo S., Cuppen H. M., Romanzin C., van Dishoeck E. F., Linnartz H., 2008, ApJ, 686, 1474
Ioppolo I., Fedoseev G., Lamberts T., Romanzin C., Linnartz H., 2013, Rev. Sci. Instrum., 84, 073112
Itikawa Y., Mason N., 2005, J. Phys. Chem. Ref. Data, 34, 1
Jung K.-H., Park S.-C., Kim J.-H., Kang H., 2004, J. Chem. Phys., 121, 2758
Jørgensen J. K., Schöier F. L., van Dishoeck E. F., 2002, A&A, 389, 908
Karssemeijer L. J., Ioppolo S., van Hemert M. C., van der Avoird A., Allodi M. A., Blake G. A., Cuppen H. M., 2014, ApJ, 781, 16
Kim J.-H., Kim Y.-K., Kang H., 2009, J. Chem. Phys., 131, 044705
Launhardt R. et al., 2013, A&A, 551, A98
Lee C.-W., Lee P.-R., Kim Y.-K., Kang H., 2007, J. Chem. Phys., 127, 084701
Miyauchi N., Hidaka H., Chigai T., Nagaoka A., Watanabe N., Kouchi A., 2008, Chem. Phys. Lett., 456, 27
Moon E.-S., Yoon J., Kang H., 2010, J. Chem. Phys., 133, 044709
Morbidelli A., Chambers J., Lunine J. I., Petit J. M., Robert F., Valsecchi G. B., Cyr K. E., 2000, Meteorit. Planet. Sci., 35, 1309
Muralidharan K., Deymier P., Stimpfl M., de Leeuw N. H., Drake M. J., 2008, Icarus, 198, 400
Nagaoka A., Watanabe N., Kouchi A., 2005, ApJ, 624, L29
Nomura H., Millar T. J., 2005, A&A, 438, 923
O'Brien D. P., Walsh K. J., Morbidelli A., Raymond S. N., Mandell A. M., 2014, Icarus, 239, 74
Oba Y., Miyauchi N., Hidaka H., Chigai T., Watanabe N., Kouchi A., 2009, ApJ, 701, 464
Oxley S. P., Zahn C. M., Pursell C. J., 2006, J. Phys. Chem. A, 110, 11064
Palumbo M. E., 2006, A&A, 453, 903
Park S.-C., Jung K.-H., Kang H., 2004, J. Chem. Phys., 121, 2765
Ratajczak A., 2012, PhD Thesis, Université de Grenoble
Ratajczak A., Quirico E., Faure A., Schmitt B., Ceccarelli C., 2009, A&A, 496, L21
Ratajczak A., Taquet V., Kahane C., Ceccarelli C., Faure A., Quirico E., 2011, A&A, 528, L13
Rodgers S. D., Charnley S. B., 2002, MNRAS, 330, 660
Schöier F. L., Jørgensen J. K., van Dishoeck E. F., Blake G. A., 2002, A&A, 390, 1001
Souda R., Kawanowa H., Kondo M., Gotoh Y., 2003, J. Chem. Phys., 119, 6194
Straub H. C., Lindsay B. G., Smith K. A., Stebbings R. F., 1998, J. Chem. Phys., 108, 109
Thornton C., Khatkale M. S., Devlin J. P., 1981, J. Chem. Phys., 75, 5609
Tielens A. G. G. M., 1983, A&A, 119, 177
Tielens A. G. G. M., 2013, Rev. Mod. Phys., 85, 1021
Uras-Aytemiz N., Joyce C., Devlin J. P., 2001, J. Chem. Phys., 115, 9835
van der Tak F. F. S., van Dishoeck E. F., Evans N. J., II, Blake G. A., 2000, ApJ, 537, 283
Vastel C. et al., 2010, A&A, 521, L31
Walsh C., Millar T. J., Nomura H., 2010, ApJ, 722, 1607
Watanabe N., Kouchi A., 2002, ApJ, 571, L173
Wooldridge P. J., Devlin J. P., 1988, J. Chem. Phys., 88, 3086

This paper has been typeset from a TEX/LATEX file prepared by the author.